Frustrated local-moment models for iron pnictide magnetism

Burkhard Schmidt, Mohammad Siahatgar, and Peter Thalmeier
Max-Planck-Institut für Chemische Physik fester Stoffe, 01187 Dresden, Germany
(Received 19 November 2009; revised manuscript received 15 January 2010; published 1 April 2010)

The low-energy spin excitations of the Fe pnictide parent compounds have been determined by inelastic neutron scattering and interpreted within the local moment $J_{1a,b}$-J_2 Heisenberg model with orthorhombic symmetry. This has led to alternative exchange models that strongly differ in the size of anisotropy. Although the compounds are itinerant the localized spin model can explain basic features of the excitations. The inherent frustration of this model leads to quantum fluctuations and possible moment reduction. We investigate this question in detail using spin-wave approximation and partly exact diagonalization Lanczos calculations for finite clusters. We find that the orthorhombic anisotropy stabilizes the columnar antiferromagnetic phase and its moment. For the exchange models proposed from inelastic neutron scattering we can exclude a strong influence of frustration on the moment size. We also investigate dependence of magnetization and susceptibility on field and temperature.

DOI: 10.1103/PhysRevB.81.165101 PACS number(s): 75.10.Jm, 75.30.Cr, 75.30.Ds

I. INTRODUCTION

The discovery of Fe pnictide superconductors has given new impetus to study the interrelation between magnetic and superconducting instabilities in condensed matter. Previous investigation of strongly correlated heavy-fermion and cuprate compounds have also shown this connection. However, unlike those compounds the pnictides are only moderately correlated[1] and in contrast to cuprates already the parent compounds are metallic. At lower temperatures they exhibit a structural phase transition from tetragonal to orthorhombic symmetry and simultaneously or subsequently show magnetic order.[2,3] For 122 and 1111 compounds the latter is found to be of the columnar antiferromagnetic (AF) type in the FeAs planes corresponding to wave vector $\mathbf{Q}=(\pi,0)$ which is equal to the nesting vector of hole and electron Fermi-surface pockets obtained from density-functional calculations of the electronic structure. This commensurate magnetic structure is stable even for a considerable range of dopings.[4,5] However it was noticed[4,5] that the size of the staggered moment depends strongly on the details of the calculation, especially on the out-of-plane position of As atoms, and is much larger as the experimental values obtained from neutron diffraction which is less than $1\mu_B$ per Fe. The moments are oriented parallel to the ordering wave vector which is aligned to the long (a) axis.

On the other hand the results of inelastic neutron scattering (INS) on the low-energy spin excitations have shown that they may be successfully described within a localized Heisenberg model that includes interactions up to next nearest neighbors, i.e., exchange bonds along the sides and diagonals of the FeAs layers.[6–10] Therefore the localized Heisenberg model is of the anisotropic $J_{1a,b}$-J_2 type with different exchange constants along the orthorhombic a, b axes. The local-moment picture has a further interesting aspect: Depending on the ratios $J_{1a,b}/J_2$ the magnetism may exhibit frustration which can strongly reduce the size of the ordered moment. As mentioned above the observed moments are much smaller than the calculated ones. Experimentally they vary from $0.36\mu_B$ in LaFeAsO to $1\mu_B$ in $SrFe_2As_2$ whereas local-density approximation (LDA) calculations give $1.9\mu_B$ (Ref. 11) and $1.7\mu_B$,[5] respectively, if the experimental values for the As positions are used. This translates to a relative moment reduction factor of 0.19–0.59. Within a model that includes only spin degrees of freedom one may conjecture that magnetic frustration and associated enhanced quantum fluctuations are the source of the strongly reduced ordered moments in the Fe pnictides. Such an idea, however needs to be treated with care. Firstly frustration itself is not a well defined concept for itinerant spins but rather refers to the local-moment model. If the latter is indeed used the extent of frustration depends crucially on the ratios of exchange constants and their anisotropies.

No consensus on the proper exchange model in the local-moment picture of Fe pnictides has emerged. Basically two proposals, both from INS (Refs. 6–10) and local-density calculations[4,5] have been made: in the first choice $J_{1b}\simeq J_{1a}$, in the second one $|J_{1b}|\ll J_{1a}$. In principle, this will lead to very different dispersion for wave vectors along the b^* axis in the two cases which may be checked experimentally. But the case remains undecided so far. The second very anisotropic case (J_{1b} was even reported slightly ferromagnetic[5]) is hard to understand in terms of a small tetragonal-to-orthorhombic structural distortion with $(a-b)/a\simeq 0.5\times 10^{-2}$. This indicates that the exchange constant should not be interpreted as bond exchange energies. Rather they are fit parameters obtained from mapping the total LDA energy with spiral magnetic structure to the classical ground-state energy of a localized Heisenberg model.[4,5]

One important motivation why a localized model is nevertheless worthwhile to study was provided by the INS results. In a metal one would naively expect that spin waves with larger wave vectors should quickly become overdamped when they merge with the continuum of particle-hole excitations. In fact it was found that well-defined spin waves exist throughout the Brillouin zone[10] giving support for the local-moment picture. Even in weakly correlated $3d$-compounds local moments may be stabilized due to Hund's rule coupling in a multiorbital case such as Fe pnictides as has been shown in Ref. 12. This is not unlike the situation in elemental Fe ferromagnetism where it was found that Hund's rule ex-

TABLE I. Fe pnictide moment $\mu=2S\mu_B$ and exchange interactions (in millielectron volt) from experiment (top, 1–5) and theory (bottom, 6–8). Here J_c is the average exchange energy scale and θ,ϕ are anisotropy and frustration angles [Eq. (5)]. The first column holds the labels used in Fig. 1 (letters) and Fig. 6 (letters and numbers).

	System	Ref.	S	SJ_{1a}	SJ_{1b}	SJ_2	SJ_c	ϕ/π	θ/π
1	$CaFe_2As_2$	7		41	10	21	36	0.19	0.08
C	$CaFe_2As_2$	9	0.4	24–37	7–20	28–34	33–45	0.29	0.13
D	$CaFe_2As_2$	10	0.22	49.9	−5.7	18.9	53.7	0.11	−0.04
B	$BaFe_2As_2$	6	0.28	17.5	17.5	35	39.1	0.35	0.25
5	$BaFe_2As_2$	6	0.54	36	−7	18	31.6	0.19	−0.06
6	$CaFe_2As_2$	5	0.75	27.4	−2.1	14.5	24.3	0.20	−0.02
7	$BaFe_2As_2$	5	0.84	36.1	−2.6	12.0	38.0	0.10	−0.02
8	$SrFe_2As_2$	5	0.84	35.3	2.2	13.4	28.4	0.16	0.02

change stabilizes the local moments.[13,14] In fact spin waves in elemental fcc Fe also exist throughout the Brillouin zone and may be described by a localized Heisenberg model although Fe is a good metal.[15] The itinerant nature of magnetism in the Fe pnictides does not by itself exclude that a local-moment model is a good starting point for studying the low-lying spin excitations. Further support for this conjecture was given by functional renormalization group calculations for the isotropic ($J_{1a}=J_{1b}=J_1$) model.[16] Starting from a multiorbital extended Hubbard model it was shown that the J_1-J_2 model is a valid description for the dominant low-energy correlations for a wide range of parameters. Coexistence models for both localized and itinerant moments in the pnictides have been proposed in Refs. 17 and 18.

Extended models including orbital degrees of freedom within a localized Kugel-Khomskii-type approach have been proposed in Refs. 19–22. In this case the ground state can exhibit orbital order which may lead to effective orthorhombic exchange anisotropy and low-ordered moment. Furthermore itinerant multiorbital models,[23–25] also including the effect of orbital order[12,26,27] for the magnetic ground state have been proposed.

The INS experiments[6–10] were interpreted within models including only spin degrees of freedom. Since we want to refer the exchange parameters found there we also restrict to these type of models. In this work we have made a systematic survey of the anisotropic (orthorhombic) two-dimensional (2D) $J_{1a,b}$-J_2 Heisenberg model. Our main subject is to examine carefully to which extent the "frustration" of nearest- and next-nearest exchange constants in this model plays a role in the reduction in the staggered moment as observed in neutron diffraction. For that purpose we are using both analytical spin-wave calculations and numerical Lanczos method for finite clusters of the 2D rectangular lattice. In the central part we investigate the evolution of the staggered moment, reduced by quantum fluctuations as function of the frustration and anisotropy ratios. This allows us to make a quantitative evaluation of the importance of frustration in the local-moment model for Fe pnictides by comparing with the results for the experimental exchange constants. The isotropic model with $J_{1a,b}=J_1$ has been studied previously within various approximations[28,29] and has also been extended including interlayer coupling.[30,31] Spin waves for the anisotropic model in zero field are also discussed in Ref. 32.

In Sec. II we introduce the localized spin model for the 2D orthorhombic Fe pnictide layers and discuss its parameterization. In Sec. III we calculate the ground-state energy and phase diagram of the model and the corresponding location of known Fe pnictide compounds. The reduction in the ordered moment by quantum fluctuations using spin-wave expansion is discussed in detail in Sec. IV. The effect of an external field in the anisotropic model is addressed in Sec. V. Finally Sec. VI gives the summary and conclusion.

II. LOCALIZED SPIN MODELS FOR 2D RECTANGULAR LATTICE

We start from a localized spin model with effective spin size $S=1/2$. The latter is suggested by INS and LDA results given in Table I which are compatible with this value. A stronger argument is given by the Gutzwiller approach to the multiorbital Hubbard model[12] which suggests that $2S\simeq 1$ for reasonable model parameters.

The orthorhombic symmetry allows for different nearest-neighbor (nn) exchange parameters $J_{1a,b}$, however the extreme difference for some parameter sets in Table I can hardly be justified by the simple effect of exchange striction on nn exchange caused by the orthorhombic distortion. As mentioned above, a more likely source of large exchange anisotropy is the presence of underlying orbital order which may appear simultaneously with magnetic order. However a quantitative prediction of the amount of anisotropy seems difficult. Due to the large differences in the proposed exchange parameters we treat the anisotropy as a free parameter.

INS results also show the existence of a small spin gap of the order $\simeq 10$ meV. For a $S=1/2$ system this can most easily be modeled by a uniaxial out-of-plane *spin-space* exchange anisotropy which will be included in the model for completeness but not discussed in detail. Further insight in the underlying frustrated exchange model may be gained from field dependence of magnetization and susceptibility as has been shown for a different class of compounds.[33,34]

Therefore we also include a Zeeman term in the model.

The effective localized spin Hamiltonian we shall discuss in this paper then has the form

$$\mathcal{H} = \sum_{\langle ij \rangle} \vec{S}_i J_{ij} \vec{S}_j - g\mu_B \vec{H} \sum_i \vec{S}_i, \tag{1}$$

where the sum in the first term extends over bonds $\langle ij \rangle$ connecting sites i and j. We assume an interaction in spin space of the form

$$J_{ij} = \mathrm{diag}(J_{ij}^{\perp}, J_{ij}^{\perp}, J_{ij}^{z}). \tag{2}$$

To conserve U(1) symmetry, the magnetic field points into the z direction defined by the anisotropy introduced above. Suppressing the direction index we set

$$J_{ij} = \begin{cases} J_{1a} & \text{if } \vec{R}_j = \vec{R}_i \pm \vec{e}_x \\ J_{1b} & \text{if } \vec{R}_j = \vec{R}_i \pm \vec{e}_y \\ J_2 & \text{if } \vec{R}_j = \vec{R}_i \pm \vec{e}_x \pm \vec{e}_y, \end{cases} \tag{3}$$

i.e., we restrict Eqs. (1) and (2) to nearest- and next-nearest-neighbor exchange on a rectangular lattice. For the discussion of the complete phase diagram of this Hamiltonian, we use a more convenient parameterization of the exchange terms and write

$$J_{1a} = \sqrt{2} J_c \cos\phi \cos\theta,$$

$$J_{1b} = \sqrt{2} J_c \cos\phi \sin\theta,$$

$$J_2 = J_c \sin\phi,$$

$$J_c = \sqrt{\frac{1}{2}(J_{1a}^2 + J_{1b}^2) + J_2^2}, \tag{4}$$

introducing an overall energy scale J_c (this should not be confused with J^z), a frustration angle ϕ, and an anisotropy parameter θ. For $\theta = \pi/4$, the above Hamiltonian reduces to the square-lattice case ($J_{1a} = J_{1b}$) investigated before, e.g., in Refs. 33–35 for V oxides.

III. CLASSICAL PHASES AND GROUND-STATE ENERGIES

For the isotropic model ($\theta = \pi/4$) these are well known and serve as starting point for discussing frustration effects. We first find out how their energies and existence regions are modified for the general anisotropic case with $-1 < \theta/\pi < 1$. On each site i, we introduce a local coordinate system, where the z' axis is oriented parallel to the local magnetic moment, and we have

$$\begin{pmatrix} S_i^x \\ S_i^y \\ S_i^z \end{pmatrix} = \begin{pmatrix} \cos(\vec{Q}\vec{R}_i) & -\sin(\vec{Q}\vec{R}_i) & 0 \\ \sin(\vec{Q}\vec{R}_i) & \cos(\vec{Q}\vec{R}_i) & 0 \\ 0 & 0 & 1 \end{pmatrix} \begin{pmatrix} \cos\Theta & 0 & -\sin\Theta \\ 0 & 1 & 0 \\ \sin\Theta & 0 & \cos\Theta \end{pmatrix} \times \begin{pmatrix} S_i^{x'} \\ S_i^{y'} \\ S_i^{z'} \end{pmatrix} \tag{5}$$

with the ordering vector $\vec{Q}$ in the xy plane perpendicular to the magnetic field which points along the z axis. At finite values of $\vec{H}$, the spins form an umbrellalike structure around the direction of $\vec{H}$; the respective canting angle Θ (not to be confused with the anisotropy parameter θ) is measured relative to the field direction (global z axis); $\Theta = 0$ corresponds to the fully polarized state, and $\Theta = \pi/2$ to the state with vanishing magnetic field.

With $h = g\mu_B H$, the classical Hamiltonian then reads

$$\mathcal{H}_{\mathrm{cl}} = NS^2 \left[J_{\perp}(\vec{Q}) + A(0)\cos^2\Theta - \frac{h}{S}\cos\Theta \right], \tag{6}$$

where we have introduced the Fourier transform

$$J_{\alpha}(\vec{k}) = \frac{1}{N}\sum_{\langle ij \rangle} J_{ij}^{\alpha} e^{-i\vec{k}(\vec{R}_i - \vec{R}_j)} = \frac{1}{2}\sum_n J_n^{\alpha} e^{-i\vec{k}\vec{R}_n} \tag{7}$$

for $\alpha = \{\perp, z\}$ and the last sum runs over all bonds n connecting a fixed site i with its neighbors. The coefficient $A(0) = A(\vec{k}=0)$ is defined by

$$A(\vec{k}) = J_z(\vec{k}) + \frac{1}{2}[J_{\perp}(\vec{k}+\vec{Q}) + J_{\perp}(\vec{k}-\vec{Q})] - 2J_{\perp}(\vec{Q}). \tag{8}$$

The reason for defining $A(\vec{k})$ in this way will become clear later in Sec. IV. Minimizing Eq. (6) with respect to Θ, we get the classical canting angle Θ_c via

$$\cos\Theta_c = \frac{h}{2SA(0)}, \tag{9}$$

and Eq. (6) reads

$$\mathcal{H}_{\mathrm{cl}} = NS^2[J_{\perp}(\vec{Q}) - A(0)\cos^2\Theta_c]. \tag{10}$$

Minimizing this Hamiltonian with the exchange parameters from Eq. (3) with respect to the components of $\vec{Q}$ leads to the four well-known classical phases with ordering vectors

$$\vec{Q} = \begin{cases} 0 & \text{ferromagnet(FM)} \\ (\pi/a, \pi/b) & \text{Néel antiferromagnet(NAF)} \\ (\pi/a, 0) & \text{columnar AF along } a\text{(CAFa)} \\ (0, \pi/b) & \text{columnar AF along } b\text{(CAFb)}. \end{cases} \tag{11}$$

The minimization condition reduces to $\partial J_{\perp}(\vec{Q})/\partial\vec{Q} = 0$ and is thus field independent and depends on the transverse exchange parameters only. The classical ground-state energies are

$$E_{\rm gs}^{\rm cl} = NS^2 \begin{cases} J_{1a}^{\perp} + J_{1b}^{\perp} + 2J_2^{\perp} & \text{FM} \\ 2J_2^{\perp} - (J_{1a}^{\perp} + J_{1b}^{\perp}) + [2(J_2^{\perp} - J_2^z) - (J_{1a}^{\perp} + J_{1a}^z) - (J_{1b}^{\perp} + J_{1b}^z)]\cos^2\Theta_c & \text{NAF} \\ J_{1b}^{\perp} - (J_{1a}^{\perp} + 2J_2^{\perp}) + [(J_{1b}^{\perp} - J_{1b}^z) - (J_{1a}^{\perp} + J_{1a}^z) - 2(J_2^{\perp} + J_2^z)]\cos^2\Theta_c & \text{CAFa} \\ J_{1a}^{\perp} - (J_{1b}^{\perp} + 2J_2^{\perp}) + [(J_{1a}^{\perp} - J_{1a}^z) - (J_{1b}^{\perp} + J_{1b}^z) - 2(J_2^{\perp} + J_2^z)]\cos^2\Theta_c & \text{CAFb}, \end{cases} \tag{12}$$

where $\cos\Theta_c = h/h_s$, and the critical or saturation fields for the nonuniform phases are given by Eq. (9),

$$\frac{h_s}{2S} = J_{1a}^z + J_{1b}^z + 2J_2^z - \begin{cases} 2J_2^{\perp} - (J_{1a}^{\perp} + J_{1b}^{\perp}) & \text{NAF} \\ J_{1b}^{\perp} - (J_{1a}^{\perp} + 2J_2^{\perp}) & \text{CAFa} \\ J_{1a}^{\perp} - (J_{1b}^{\perp} + 2J_2^{\perp}) & \text{CAFb}. \end{cases} \tag{13}$$

The minimization condition contains an additional extremal solution having an incommensurate wave vector given by

$$\cos Q_x a = -\frac{J_{1b}}{2J_2}, \quad \cos Q_y b = -\frac{J_{1a}}{2J_2}, \tag{14}$$

with a ground-state energy

$$E_{\rm gs}^{\rm cl} = -\frac{J_{1a}J_{1b}}{8J_2}. \tag{15}$$

However, this energy for the incommensurate wave vector is always higher than or equal to the energy in Eq. (12) of the commensurate ground state corresponding to the values chosen for the exchange constants.

From the classical ground-state energy in Eq. (12) one may already construct the phase diagram in the ϕ, θ plane, however for the following discussions it is important to include the effect of quantum fluctuations.

IV. QUANTUM FLUCTUATIONS AND ORDERED MOMENT SIZE IN SPIN-WAVE APPROXIMATION

In the regions of the ϕ, θ plane where two or more of the classical phases become degenerate large quantum fluctuations appear and reduce or suppress the ordered moment. These are the strongly frustrated regions of the phase diagram. One may approach them to some extent by starting from the stable region and calculate the contribution of zero-point fluctuations in spin-wave approximation. This leads to an improved ground-state energy, an estimate for the reduction in the ordered moment and for the extent of the instability region where magnetic order breaks down. This program has been successfully implemented before for the isotropic case.[33,34] It will now be carried out for the more general model in order to quantify the importance of frustration and quantum fluctuations for the compounds listed in Table I.

Returning to Eq. (1) expressed in the local coordinate system introduced in Sec. III, Eq. (5), we apply a Holstein-Primakoff transformation and carry out a $1/S$ expansion, keeping terms up to first order in $1/S$. (We regard h formally as proportional to S.) Next, we apply a Fourier transformation. A detailed description of the necessary steps can be found in Appendix A. The resulting Hamiltonian is given by

$$\begin{aligned} \mathcal{H} = \mathcal{H}_{\rm cl} + NS\left[J_{\perp}(\vec{Q}) + A(0)\cos^2\Theta - \frac{h}{2S}\cos\Theta\right] \\ + \sqrt{2NS^3}\sin\Theta\left[A(0)\cos\Theta - \frac{h}{2S}\right](a_0 + a_0^{\dagger}) \\ + \frac{S}{2}\sum_{\vec{k}}\left(\left\{A(\vec{k}) - \cos^2\Theta[B(\vec{k}) + 2A(0)] + \frac{h}{S}\cos\Theta\right\}(a_{\vec{k}}^{\dagger}a_{\vec{k}} \right. \\ \left. + a_{-\vec{k}}a_{-\vec{k}}^{\dagger}) + B(\vec{k})(1 - \cos^2\Theta)(a_{\vec{k}}a_{-\vec{k}} + a_{\vec{k}}^{\dagger}a_{-\vec{k}}^{\dagger}) \right. \\ \left. + C(\vec{k})\cos\Theta(a_{\vec{k}}^{\dagger}a_{\vec{k}} - a_{-\vec{k}}a_{-\vec{k}}^{\dagger})\right), \end{aligned} \tag{16}$$

where $A(\vec{k})$ is defined in Eq. (8), and

$$B(\vec{k}) = J_z(\vec{k}) - \frac{1}{2}[J_{\perp}(\vec{k} + \vec{Q}) + J_{\perp}(\vec{k} - \vec{Q})], \tag{17}$$

$$C(\vec{k}) = J_{\perp}(\vec{k} + \vec{Q}) - J_{\perp}(\vec{k} - \vec{Q}). \tag{18}$$

Equation (16) still contains a part which is linear in the bosons with zero momentum. It occurs only in finite magnetic fields. In equilibrium, when $\Theta = \Theta_c$ [see Eq. (9)], this part vanishes, and we will drop it in the following. A subsequent Bogoliubov transformation leads to the final form

$$\mathcal{H} = \mathcal{H}_{\rm cl} + \mathcal{H}_{\rm zp} + S\sum_{\vec{k}} E(h,\vec{k})\alpha_{\vec{k}}^{\dagger}\alpha_{\vec{k}}, \tag{19}$$

where $\mathcal{H}_{\rm cl}$ is given by Eq. (10), and

$$\mathcal{H}_{\rm zp} = NSJ_{\perp}(\vec{Q}) + \frac{S}{2}\sum_{\vec{k}} E(h,\vec{k}) \tag{20}$$

is the zero-point energy contribution to the total ground-state energy $E_{\rm gs} = \mathcal{H}_{\rm cl} + \mathcal{H}_{\rm zp}$. The former corresponds to the magnon excitations described by the boson operators

$$\alpha_{\vec{k}} = u_{\vec{k}}a_{\vec{k}} + v_{\vec{k}}a_{-\vec{k}}^{\dagger}, \tag{21}$$

$$\alpha_{-\vec{k}}^{\dagger} = v_{\vec{k}}a_{\vec{k}} + u_{\vec{k}}a_{-\vec{k}}^{\dagger}. \tag{22}$$

The $\vec{k}$ sums in the equations above span the full crystallographic Brillouin zone. For the spin-wave dispersion, we obtain the expression

$$E(h,\vec{k}) = \sqrt{[A(\vec{k}) - B(\vec{k})\cos^2\Theta_c]^2 - [B(\vec{k})(1-\cos^2\Theta_c)]^2} + C(\vec{k})\cos\Theta_c. \quad (23)$$

$C(\vec{k})$ only occurs at finite magnetic fields, and because it is antisymmetric in $\vec{k}$, it does not contribute to the zero-point fluctuations.

A. Total ground-state energy

We now calculate the total ground-state energy in spin-wave approximation to determine the zero-field phase diagram. We also will give a comparison to the classical ground-state energy and the results for finite clusters obtained from the exact-diagonalization Lanczos method.

Unless explicitly mentioned otherwise, we assume $\Theta = \Theta_c$ from here on. Furthermore spin space anisotropy is ignored ($J_{ij}^{\perp} = J_{ij}^{z}$) from now on. The ground-state energy is given by the sum of the classical energy, Eq. (10) and the zero-point fluctuations of the magnons, Eq. (20), with the dispersion from Eq. (23). Explicitly we have for isotropic exchange parameters

FM: no zero-point fluctuations

$$J(\vec{Q}) = J_{1a} + J_{1b} + 2J_2,$$

$$A(\vec{k}) = 2\{J_{1a}[\cos(k_x a) - 1] + J_{1b}[\cos(k_y b) - 1] + 2J_2[\cos(k_x a)\cos(k_y b) - 1]\},$$

$$B(\vec{k}) = 0, \quad (24)$$

NAF: $\vec{Q} = (\pi, \pi)$,

$$J(\vec{Q}) = -(J_{1a} + J_{1b}) + 2J_2,$$

$$A(\vec{k}) = 2\{J_{1a} + J_{1b} + 2J_2[\cos(k_x a)\cos(k_y b) - 1]\},$$

$$B(\vec{k}) = -2[J_{1a}\cos(k_x a) + J_{1b}\cos(k_y b)], \quad (25)$$

CAFa: $\vec{Q} = (\pi, 0)$,

$$J(\vec{Q}) = J_{1b} - (J_{1a} + 2J_2),$$

$$A(\vec{k}) = 2\{J_{1a} + J_{1b}[\cos(k_y b) - 1] + 2J_2\},$$

$$B(\vec{k}) = -2[J_{1a}\cos(k_x a) + 2J_2\cos(k_x a)\cos(k_y b)]. \quad (26)$$

CAFb: $\vec{Q} = (0, \pi)$,

$$J(\vec{Q}) = J_{1a} - (J_{1b} + 2J_2),$$

$$A(\vec{k}) = 2\{J_{1a}[\cos(k_x a) - 1] + J_{1b} + 2J_2\},$$

$$B(\vec{k}) = -2[J_{1b}\cos(k_y b) + 2J_2\cos(k_x a)\cos(k_y b)]. \quad (27)$$

Figure 1 shows a contour plot of the total ground-state energy $E_{gs} = \mathcal{H}_{cl} + \mathcal{H}_{zp}$ at zero field as a function of the frustration angle ϕ and the anisotropy parameter θ. The energy unit is J_c. Four magnetic phases appear (see caption) in a symmetric pattern in the ϕ, θ plane. We present the complete phase diagram of the $J_{1a,b}$-J_2 model although only the sector $0 < \theta/\pi < 0.25$, $0 < \phi/\pi < 0.5$ seems to be relevant for the Fe pnictide class according to Table I. We notice the following characteristics of the phase diagram: (i) the ground-state energy and phase diagram are invariant under the following symmetry transformations: reflections at the lines $\theta = \pi/4$ and $-3\pi/4$ and inversion at the points $(\phi, \theta) = (\pm\pi/2, 3\pi/4)$. Both operations lead to $(J_{1a}, J_{1b}) \rightarrow (J_{1b}, J_{1a})$ with J_2 unchanged. This corresponds to an interchange of the columnar CAFa/b phases while FM and NAF are mapped identically. The classical ground-state energy has even more symmetries.

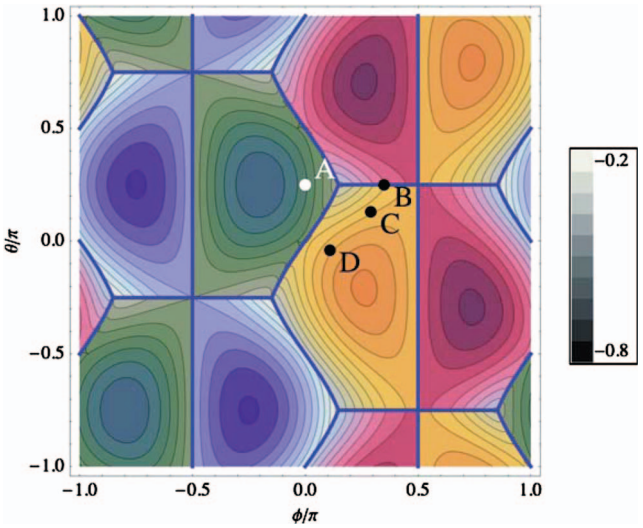

FIG. 1. (Color) Ground-state energy in linear spin-wave approximation of the frustrated Heisenberg Hamiltonian on the rectangular lattice as a function of the frustration angle ϕ and the anisotropy parameter θ. Energy unit is the overall energy scale J_c, the magnetic field is zero. The four different classical phases are labeled by color: Blue—FM, green—NAF, orange—CAFa, red—CAFb. The thick lines correspond to the classical phase boundaries, the symbols indicate the locations of the parameters used in Fig. 3 and are labeled with the corresponding character, also used in Table I. The white dot represents the standard nearest-neighbor Heisenberg model ($J_{1a} = J_{1b} = J_1, J_2 = 0$), the black dots denote experimental points for $BaFe_2As_2$ in Ref. 6 and $CaFe_2As_2$ in Refs. 9 and 10.

(ii) In the isotropic case ($\theta = \pi/4$) CAFa and CAFb are degenerate, and moving away from this symmetry line one of the two phases is selected. The stability region of the columnar phases along the frustration axis (ϕ) increases upon going away from the symmetry line $\theta = \pi/4$ while that of the neighboring NAF or FM phase decreases. Therefore CAFa/b is stabilized by the presence of a $J_{1a,b}$ anisotropy.

(iii) The exchange frustration is largest where three phases (e.g., the corner point $\theta/\pi = 0.25$, $\phi/\pi \simeq 0.15$, and $J_2/J_1 = 1/2$) or two phases (the boundary lines) meet. Therefore the degree of frustration in a given compound in Table I also depends on the size of its anisotropy. While the above corner point is strongly frustrated and in fact has no long-range order (see Sec. IV C) the point $\theta = 0$, $\phi/\pi \approx 0.15$ [$J_{1b} = 0$, close to (D) in Fig. 1] is *not* strongly frustrated but stable

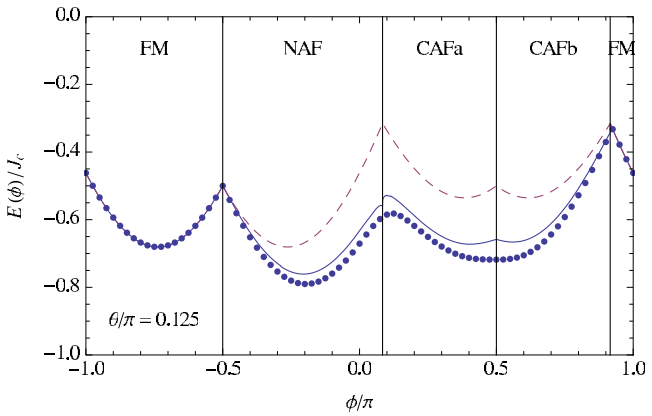

FIG. 2. (Color online) Ground-state energy as a function of the frustration angle ϕ for fixed anisotropy parameter $\theta=\pi/8$ from linear spin-wave theory (solid line) and exact diagonalization (solid dots; 24 sites). For comparison, the dashed curve shows the classical ground-state energy. Here and in subsequent plots of ϕ dependent quantities the vertical lines indicate the classical phase boundaries.

CAFa despite having $\phi/\pi \approx 0.15$ or $J_2/(J_{1a}/\sqrt{2})=1/2$.

Apart from the ferromagnet, which is an eigenstate to the full Hamiltonian, the spin-wave corrections stabilize the classical ground state, i.e., the zero-point energy in Eq. (20) is negative semidefinite for all values of ϕ and θ. As an example, Fig. 2 displays the dependence of the ground-state energy on the frustration angle ϕ obtained both from linear spin-wave theory (solid line) and from the classical model (dashed line). The plot was made with fixed anisotropy parameter $\theta=\pi/8$, corresponding to a spatial anisotropy $J_{1b}/J_{1a}=\sqrt{2}-1\approx 0.414$. For a comparison we also present the numerical results from Lanczos calculations for finite clusters of the square lattice with size $N=24$ which is quite close to the spin-wave results.

B. Spin-wave spectra

We shall now discuss the excitation spectrum of Hamiltonian (19) for some typical points in the (ϕ,θ) phase diagram, Fig. 1. In Table I, we have compiled an excerpt from the available literature on experimental and theoretical values for the exchange parameters of AFe_2As_2 compounds, where A denotes an alkaline metal. From this list, we have chosen three parameter sets, indicated by the black dots in Fig. 1, and the standard Néel antiferromagnet (white dot).

Figure 3 shows plots of the $\vec{k}$ dependence of the spin-wave excitations for different parameter sets (ϕ,θ). The parameter sets used for the plots are indicated by the symbols in Fig. 1. For simplicity, we scale $\vec{k}$ with the lattice constants and set $k_x a \to k_x$ and $k_y b \to k_y$. All plots refer to the full crystallographic Brillouin zone.

The top left spectrum (A) in Fig. 3 shows the well-known dispersion for the nearest-neighbor Heisenberg model for comparison. It has a Goldstone mode at the equivalent wave vectors $\vec{Q}=0$ and $\vec{Q}=(\pm\pi,\pm\pi)$. The low-energy dispersion $\omega(\vec{k})=SE(\vec{k})$ is linear around these points with

$$\omega(\vec{k}) = 2S\sqrt{J_{1a}+J_{1b}} \times \sqrt{(J_{1a}-2J_2)(k_x-Q_x)^2+(J_{1b}-2J_2)(k_y-Q_y)^2}. \tag{28}$$

The top-right plot (B) shows the dispersion for $(\phi,\theta)/\pi=(0.35,0.25)$, corresponding to an isotropic exchange on the border between CAFa and CAFb phases. These parameters have been determined for $BaFe_2As_2$ in Ref. 6. The Goldstone modes are at $\vec{Q}=(0,\pm\pi)$ and $\vec{Q}=(\pm\pi,0)$ and the equivalent points $\vec{Q}=0$ and $\vec{Q}=(\pm\pi,\pm\pi)$, reflecting the twofold degeneracy of the CAFa and CAFb phases. The linear dispersion around the minima is

$$\omega_a(\vec{k}) = 2S\sqrt{2J_2+J_{1a}} \times \sqrt{(2J_2+J_{1a})(k_x-Q_x)^2+(2J_2-J_{1b})(k_y-Q_y)^2} \tag{29}$$

for the CAFa phase, and

$$\omega_b(\vec{k}) = 2S\sqrt{2J_2+J_{1b}} \times \sqrt{(2J_2-J_{1a})(k_x-Q_x)^2+(2J_2+J_{1b})(k_y-Q_y)^2} \tag{30}$$

for the CAFb phase.

For $(\phi,\theta)/\pi=(0.29,0.13)$, assigned to $CaFe_2As_2$ in Ref. 9, we show the spin-wave dispersion in the bottom right plot (C) of Fig. 3. With these parameters, the system is deep inside the CAFa phase. In contrast to the isotropic case, the dispersion around $\vec{Q}^*=(0,\pm\pi)$ and $(\pm\pi,\pm\pi)$, while still being local minima (but with a quadratic $\vec{k}$ dependence), have a finite energy gap. We have $E_a(\vec{k})=0$ remaining only at the wave vectors $\vec{k}=0$ and $(\pm\pi,0)$, characteristic for the CAFa phase.

Finally, the bottom left plot (D) in Fig. 3 displays the dispersion for $(\phi,\theta)/\pi=(0.11,-0.04)$. This alternative parameter set was proposed in Ref. 10 for $CaFe_2As_2$. The local minima at $\vec{Q}^*=(0,\pm\pi)$ and $(\pm\pi,\pm\pi)$ discussed in the previous paragraph have almost disappeared, the dispersion at the zone boundary $k_y=\pm\pi$ is flat. This property can be utilized to decide between the two apparently different parameter sets for the identical compound. In fact from this comparison it was concluded[10] that the strongly anisotropic set (D) describes the dispersion along $(0,k_y)$ much better for large wave vectors $k_y/\pi>0.5$. Since the ordering is still of the CAFa type, the Goldstone mode at $\vec{Q}=(\pm\pi,0)$ remains for the 2D model. A realistic description of the dispersion requires, however, the inclusion of interplane exchange[9,10] which leads to a finite gap at these points.[31]

C. Ordered moment

The most appropriate quantity for judging the degree of frustration in the local-moment model is the size of the ordered ground-state moment $m_s(\phi,\theta)$ relative to its size for the unfrustrated $(J_2=0)$ isotropic $(J_{1a}=J_{1b}=J_1)$ NAF state. The latter is already reduced with respect to the classical value S to $m_s^0 \sim 0.607S$. The stronger the frustration the more

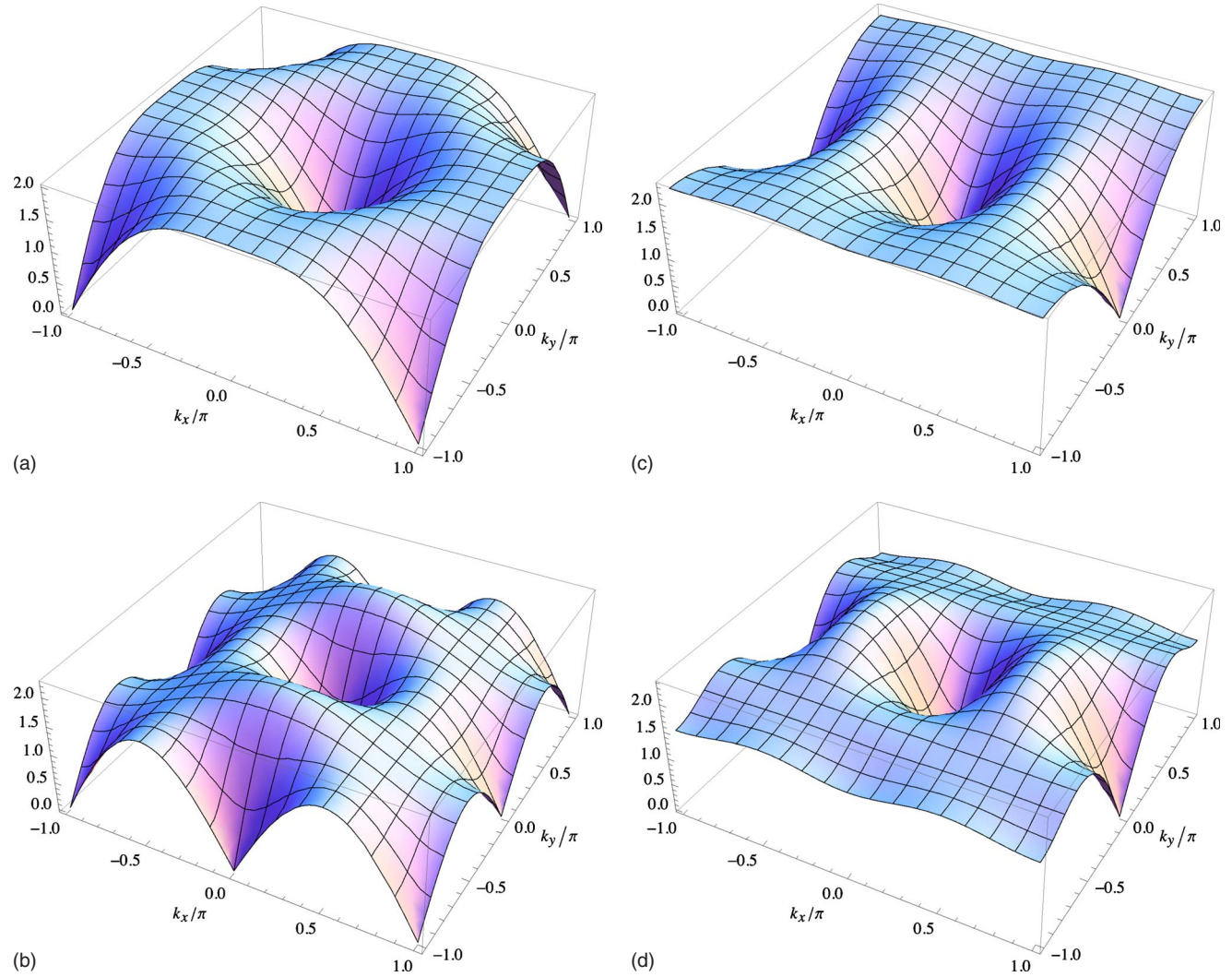

FIG. 3. (Color online) Spin-wave spectra $\omega(\vec{k})/J_c$. Clockwise from top left: (A) $(\phi,\theta)/\pi=(0,0.25)$—NAF, isotropic exchange with $J_2=0$; (B) $(\phi,\theta)/\pi=(0.35,0.25)$—CAFa/b, isotropic exchange; (C) $(\phi,\theta)/\pi=(0.29,0.13)$—inside CAFa; (D) $(\phi,\theta)/\pi=(0.11,-0.04)$–even more inside CAFa.

m_s should be reduced even below the NAF value. In the isotropic case when $J_2<0$ there is obviously no frustration and the NAF state is even stabilized. The essential question is: how large is the degree of frustration in the CAFb,b states relevant for the Fe pnictides? This question can be answered by calculating the moment reduction $m_s(\phi,\theta)/S$ in spin-wave approximation.

The ordered moment is the ground-state expectation value of the z component of the spin $\vec{S}'$ in the local coordinate system,

$$m_s = \frac{1}{N}\sum_i \langle S_i^{z'}\rangle = S - \frac{1}{N}\sum_{\vec{k}} \langle \alpha_{\vec{k}}^\dagger \alpha_{\vec{k}}\rangle = S - \frac{1}{N}\sum_{\vec{k}} v_{\vec{k}}^2. \quad (31)$$

Inserting the expression for $v_{\vec{k}}$ required to bring $\mathcal{H}$ into diagonal form (see Appendix B for a complete expression), we get

$$m_s = S\left\{1 - \frac{1}{2S}\left[\frac{1}{N}\sum_{\vec{k}} \frac{A(\vec{k}) - B(\vec{k})\cos^2\Theta_c}{E(h,\vec{k})} - 1\right]\right\}. \quad (32)$$

Due to quantum fluctuations $m_s<S$ is smaller than in the classical case, except for the ferromagnet. Near the borders of the CAFb and CAFa phases to the NAF phase, the ordered moment vanishes, indicating the failure of spin-wave theory due to strong frustrations. Also between the FM and CAF phases the latter lead to a vanishing m_s in a small region.

Figure 4 displays the behavior of $m_s=\mu/\mu_B$ as a function of the frustration angle ϕ for three different anisotropy parameters θ. The upper plot shows the isotropic case (see also Ref. 28), $\theta=\pi/4$, corresponding to $J_{1a}=J_{1b}=J_1$. Coming from the FM phase for $\phi<-\pi/2$, m_s is gradually suppressed to the well-known value $m_s^0\approx 0.3034$ at $\phi=0$ ($J_2=0$), corresponding to the NAF state of the nearest-neighbor Heisenberg model.

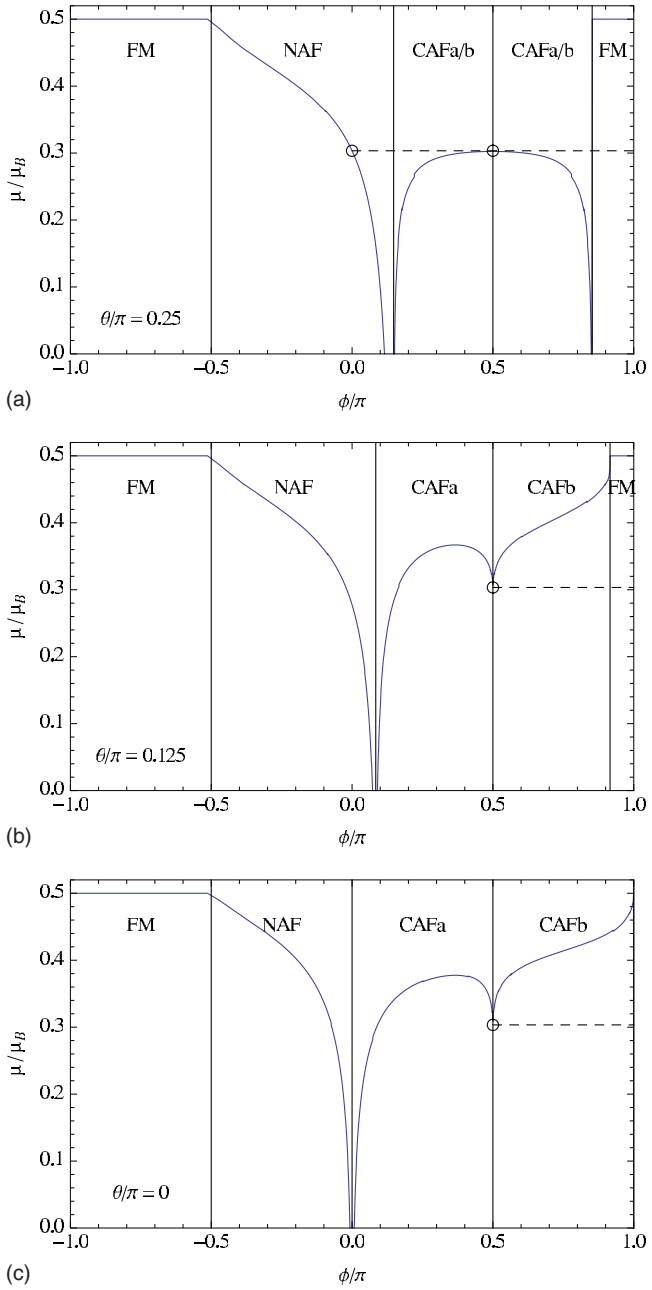

FIG. 4. (Color online) Ordered moment $m_s=\mu/\mu_B$ for fixed anisotropy parameter θ as a function of the frustration angle ϕ. Top: $\theta=\pi/4$ (isotropic case, $J_{1a}=J_{1b}$). The ordered moment vanishes for $0.1150 \lesssim \phi/\pi \lesssim 0.1508$ (NAF-CAFa/b) and $0.8491 \lesssim \phi/\pi \lesssim 0.8524$ (CAFa/b-FM crossover). Middle: $\theta=\pi/8$. The gap between NAF and CAFa is smaller but still finite, the disordered region between CAFb and FM has disappeared. Bottom: $\theta=0$, corresponding to $J_{1b}=0$. The gap $m_s=0$ appears for $-0.00727 \lesssim \phi/\pi \lesssim 0.00775$. The dashed horizontal line in the three plots denotes the value $m_s \approx 0.3034$ obtained for the standard Heisenberg model with $J_{1a}=J_{1b}$ and $J_2=0$.

Increasing ϕ towards the NAF-CAFa/b boundary further reduces m_s, until at $\phi/\pi \approx 0.1150$ (where $J_2/J_1 \approx 0.3779$), the ordered moment vanishes. The classical CAFa/b-NAF border is given by $J_2/J_1=1/2$, or $\phi/\pi \approx 0.1476$. Soon after entering the CAFa/b regime, at $\phi/\pi \approx 0.1508$ or $J_2/J_1 \approx 0.5129$, m_s becomes finite again and grows rapidly towards an almost constant value $m_s \approx m_s(J_1=0)$.

At $J_1=0$ or $\phi=\pi/2$, the lattice can be subdivided into two noninteracting sublattices with a nearest-neighbor interaction $J=J_2$, therefore we must have $m_s(\phi=\pi/2) \equiv m_s(\phi=0)$. This is indicated by the dashed horizontal line which illustrates that throughout most of the CAF region the moment reduction is almost the same as that of the unfrustrated NAF. In fact for $\phi=\pi/2$ the CAF moment is *stabilized* by quantum fluctuations which orient the moments of the two sublattices parallel. This is the so-called "order by disorder" mechanism.

The behavior of the ordered moment in the CAFa/b phase is independent of the sign of J_1 and therefore symmetric around $\phi=\pi/2$. Reaching the border to the FM phase, m_s sharply drops back to zero at $\phi/\pi \approx 0.8492$ or $J_2/J_1 \approx -0.5129$. The CAFa/b-FM border is given by $J_2/J_1=-1/2$, or $\phi/\pi \approx 0.8524$. At this border, m_s immediately jumps to the saturation value $m_s=1/2$ in the FM phase.

Now we turn to the anisotropic case, $\theta \neq \pi/4$. The lower two plots of Fig. 4 show m_s for $\theta=\pi/8$, corresponding to $J_{1b}/J_{1a}=\sqrt{2}-1 \approx 0.41$, and the fully anisotropic case $\theta=0$, meaning $J_{1b}=0$. For $\phi/\pi < 1/2$, the overall behavior of m_s is similar to the isotropic case: After leaving the FM regime, m_s is suppressed down to zero, and becomes finite again after the crossover to the CAFa phase. However, there are two quantitative differences: firstly, the region where $m_s=0$ is smaller than for $\theta=\pi/4$. Secondly and most importantly inside the columnar AF phases, the ordered moment is restored to even larger values than for isotropic exchange.

Exactly at $\phi=\pi/2$, we have $J_{1a}=J_{1b}=0$, and m_s shows a dip with the universal value $m_s \approx 0.3034$ of the nearest-neighbor Heisenberg model, indicated by the dashed lines in the plots. For any value of θ, at this point only J_2 is finite, and the same argument as for the isotropic case applies; we must have $m_s(\phi=\pi/2) \equiv m_s(\phi=0)$ for arbitrary ratios J_{1b}/J_{1a}.

In contrast to the isotropic case, the symmetry around the point $\phi=\pi/2$ is lost, and m_s is restored in the CAFb phase towards the saturation value upon entering the FM phase. There is no region around the CAFb/FM border where m_s is suppressed as in the isotropic case.

A vanishing ordered moment implies that, at least within our approximation, the order parameter for the corresponding classical phase is destroyed by quantum fluctuations. Historically this was one of the first indications of the appearance of an intermediate phase without magnetic order and our findings suggest that the well-known disordered phase for the isotropic J_1-J_2 model for AF exchange couplings extends to the whole range of anisotropic interactions with arbitrary ratios J_{1b}/J_{1a}.

This is *not* the case for the CAFa/b-FM crossover, where numerically already at a deviation $\Delta\theta/\theta < 0.01$ from the isotropic value $\theta=\pi/4$ the ordered moment remains well-defined around the classical CAFa/b-FM transition point. Figure 5 illustrates this behavior: the plot shows the ordered moment as a function of the anisotropy parameter for fixed frustration angle $\phi/\pi=0.8520$ in the whole phase diagram. The two sharp dips at $\theta=-3\pi/4$ and $\pi/4$ correspond to the disordered regimes at the CAFa/b-NAF corner and the CAFa/b-FM corner in the phase diagram, respectively. At the

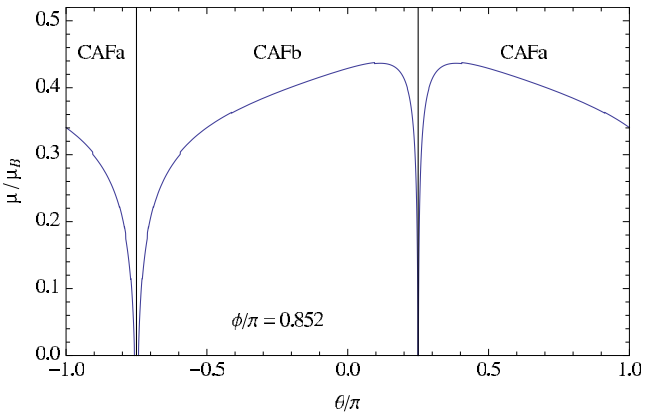

FIG. 5. (Color online) Ordered moment m_s for $\phi/\pi=0.852$ as a function of the anisotropy parameter θ. The frustration angle is chosen such that in the isotropic case ($\theta=\pi/4$), the system is in the disordered regime at the CAFa/b-FM corner.

CAFa/b-FM corner around $\theta=\pi/4$, we have $m_s=0$ only for a tiny range $0.2493 \lesssim \theta/\pi \lesssim 0.2507$. However, the precise relation to the extension of the disordered phase around this corner for finite orthorhombic anisotropy remains unclear.

In summary, if one regards the lower two panels in Fig. 4 representing the anisotropic case one observes a remarkable fact: the moment reduction by quantum fluctuation in the CAFa/b phases is *less* than in the *unfrustrated* simple nearest-neighbor NAF phase (open circle), except for a very small region close to the strongly frustrated CAFa/NAF boundary line. If one compiles the reduced moments $m_s(\phi,\theta)$ for the proposed parameter sets of Fe-pnictide compounds (Table I) as shown in Fig. 6 it is obvious that in most cases the moment reduction by quantum fluctuations for the proposed CAFa models is less than in the simple nearest-neighbor NAF

This result is in part due to the stabilization of the moment due to the effect of the anisotropy as visible from Fig. 4 which extends the stable range of ϕ for the CAFa phase in Fig. 1. In fact the frustration angle for $BaFe_2As_2$ (D) is rather

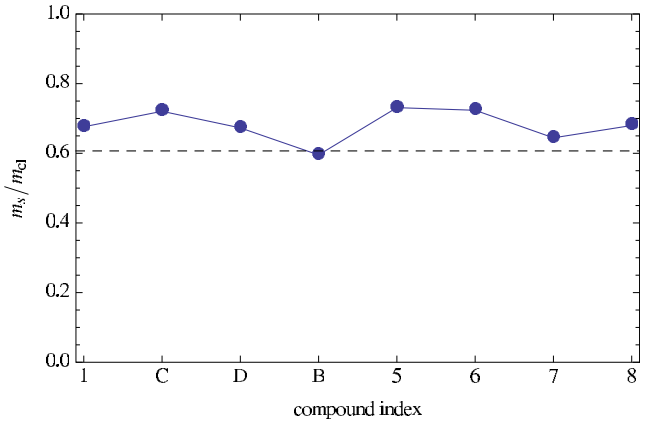

FIG. 6. (Color online) Ordered moments $m_s(\phi,\theta)$ normalized to the classical constant $m_{cl}=S$ for the compounds listed in Table I calculated with Eq. (32). The dashed horizontal line indicates $m_s(\phi=0,\theta=\pi/4)$ for the simple $J_2=0$, $J_{1a}=J_{1b}$ nearest-neighbor Heisenberg model (point A in Fig. 1).

close to the strongly frustrated value $\phi/\pi=0.15$ of the *isotropic* ($\theta/\pi=0.25$) model; nevertheless it is at a considerable distance from the anisotropic CAFa/NAF instability line and hence shows only moderate moment reduction. Therefore from Fig. 6 we conclude that frustration/quantum fluctuation effects within a local-moment picture may not be used to explain the surprisingly small ordered moment of the pnictides. We note, however that this conclusion does not invalidate the usefulness of the $J_{1a,b}$-J_2 local-moment model for the interpretation of INS spin-wave results. In classical (linear) spin-wave theory only the products SJ_i enter the spin-wave velocity and dispersion $SE(\vec{k})$ and therefore the shape of the dispersion does not depend on the size of the staggered moment as long as this approximation is reasonable.

V. FIELD-DEPENDENT PROPERTIES OF THE $J_{1a,b}$-J_2 MODEL

It has been shown that high-field magnetization (up to the saturation field h_s) is an excellent way to investigate the isotropic J_1-J_2 model[33,34] because the degree of exchange frustration determines the characteristic nonlinearity of the magnetization curve. This is especially true for the parameter region where the CAF phase is realized. One should remark however that in the undoped Fe pnictides the energy scale of $J_c \simeq 5\times 10^2$ K is too large to reach the high-field region. However it might be feasible for some of the doped Fe pnictides where the ordering temperature T_m and hence J_c are strongly reduced, provided that doping in the spacing layers does not impede the usefulness of the $J_{1a,b}$-J_2 model for the spin excitations in the FeAs layers.

A. Magnetization at high fields

The total magnetization of the system is the ground-state expectation value of the z component of the spin $\vec{S}$ in the global coordinate system,

$$m = \frac{1}{N}\sum_i \langle S_i^z \rangle. \tag{33}$$

Since this is just the projection of the ordered magnetic moments onto the field direction, we can also write

$$m = m_s \cos\Theta. \tag{34}$$

Here, Θ is *not* the classical canting angle Θ_c [this would describe the field dependence of the classical spin system, i.e., a straight line $m(h)=S(h/h_s)$] but rather must include the first-order corrections from linear spin-wave theory. We thus have to regard Θ as independent variable again, return to the Hamiltonian given by Eq. (19) before the replacement $\Theta \to \Theta_c$, and minimize its corresponding ground-state energy with respect to Θ.

Since $1/S$ corrections are already included in the ground-state energy $E_{gs}(\Theta_c)=\mathcal{H}_{cl}+\mathcal{H}_{zp}$ of the linear spin-wave (LSW) Hamiltonian given by Eqs. (10), (19), (20), and (23), we can equivalently use the definition of the total magnetization per site as the negative field derivative of $E_{gs}(\Theta_c)$,

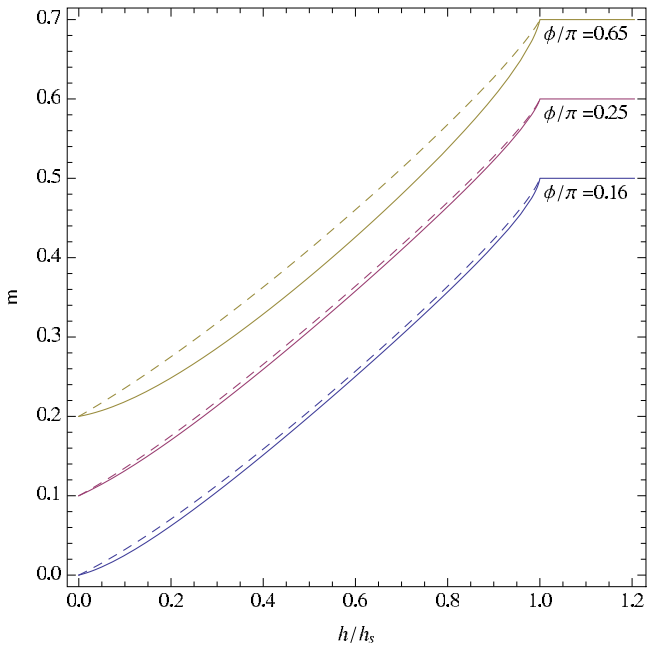

FIG. 7. (Color online) Uniform magnetic moment m per site as a function of the applied magnetic field h/h_s at three different frustration angles in the CAF phases, $\phi/\pi=0.16$ (near NAF), 0.25 (CAFa), and 0.65 (CAFb near FM). Between each pair of adjacent curves an offset $\Delta m=0.1$ is inserted. The solid lines denote the field dependence in the isotropic case, $\theta=\pi/4$, the dashed lines denote the maximally anisotropic case, $\theta=0$.

$$m = -\frac{1}{N}\frac{\partial}{\partial h}E_{\mathrm{gs}}(\Theta_c) \tag{35}$$

with Θ_c given by Eq. (9). The result is

$$m = S\frac{h}{h_s}\left[1 + \frac{1}{2S}\frac{1}{N}\sum_{\vec{k}}\frac{B(\vec{k})(A(\vec{k}) - B(\vec{k}))}{A(0)E(h,\vec{k})}\right] \tag{36}$$

(see Appendix C for details).

Figure 7 displays three sets of curves of $m(h)$ for different frustration angles. The magnetic field is normalized to the respective saturation field. The solid curves show the field dependence of the induced moment m in the isotropic case $\theta=\pi/4$, $J_{1a}=J_{1b}$, and the dashes curves show the same quantity in the maximally anisotropic case $\theta=0$ or $J_{1b}=0$.

Deep inside the ordered phases (well separated from phase boundaries), the first-order corrections to the total moment are small, as indicated by the small bending of $m(h)$ for $\phi/\pi=0.25$ (middle curve) in Fig. 7. It is only near the crossover between adjacent different phases, where corrections become strong, and the field dependence of the magnetization differs significantly from the classical behavior, as shown in $m(h)$ for $\phi/\pi=0.65$ with isotropic exchange constants.

Introducing an anisotropy generally reduces the quantum corrections leading to the nonlinear magnetization (dashed curves). According to Table I the Fe pnictides are not close to the phase boundaries, therefore the effect of the anisotropy on the nonlinear magnetization curves is not very prominent as indeed suggested by Fig. 7.

B. Magnetic susceptibility at low fields

Another sensitive probe to the degree of frustration is the low-field uniform susceptibility $\chi=\partial m/\partial h$ which may be used to obtain further insight as an alternative to the ordered moment. We obtain

$$\chi = \frac{1}{2A(0)}\left\{1 + \frac{1}{2S}\frac{1}{N}\sum_{\vec{k}}\frac{B(\vec{k})[A(\vec{k}) - B(\vec{k})]}{A(0)E(h,\vec{k})} + \frac{1}{S}\cos^2\Theta_c\frac{1}{N}\sum_{\vec{k}}\frac{B^2(\vec{k})[A(\vec{k}) - B(\vec{k})]^2}{A(0)E^3(h,\vec{k})}\right\}, \tag{37}$$

where the terms in brackets include the first-order corrections to the classical value,

$$\chi_{\mathrm{cl}} = \frac{1}{2A(0)} = \frac{S}{h_s} = \mathrm{const.} \tag{38}$$

In the FM regions, χ is undefined, since the system at $T=0$ is already fully polarized. In the three AF phases, χ diverges near the FM phase, apart from those areas, where already the vanishing ordered moment discussed above indicates that the ordered phase is no longer stable.

Figure 8 shows the dependence of χ on the frustration angle ϕ for three different anisotropy parameters θ. In the top of Fig. 8, the isotropic case is shown. The susceptibility diverges at the crossover from the NAF to the FM phase ($J_{1a}=J_{1b}=0, \phi/\pi=-1/2$). Around the border to the CAF phases [$\phi=\tan^{-1}(1/2)$], it vanishes and becomes undefined. Qualitatively the same happens near the border to the FM phase at $\phi=\pi-\tan^{-1}(1/2)$. Apart from shifting the classical phase boundaries, introducing an orthorhombic anisotropy generally stabilizes the magnetic CAF ground state. Therefore the "gaps" where strong frustration destroys the magnetic order are gradually closed, see the center plot of Fig. 8.

At the CAFb/FM crossover, the behavior of χ even changes to a divergence upon increasing the orthorhombic asymmetry by lowering θ. The bottom part of Fig. 8 shows χ for $J_{1b}=0$, where the gap to the FM phase is closed. This is fully compatible with the rapid stabilization of the CAFb ordered moment as function of increasing anisotropy (see. Fig. 4) at the boundary to FM.

At $\phi=\pi/2$, the ϕ dependence of the magnetic susceptibility has the same feature as the ordered moment discussed in Sec. IV C: At $\phi=\pi/2$, $J_1=0$, and we must have $\chi(\phi=0, \theta=\pi/4) \equiv \chi(\phi=\pi/2, \theta=\text{arbitrary})$, therefore a small dip appears in the orthorhombic case.

In the CAFa sector relevant for the pnictides the susceptibility has a plateau value except very close to the gap of instability. The value is almost equal to that for the unfrustrated simple nn NAF. This underlines again that quantum fluctuations due to frustration cannot explain the anomalous magnetism of Fe pnictides.

Furthermore the uniform susceptibility was found to have an unexpected temperature dependence. Within the (semi-) metallic itinerant model characterized by electron and hole

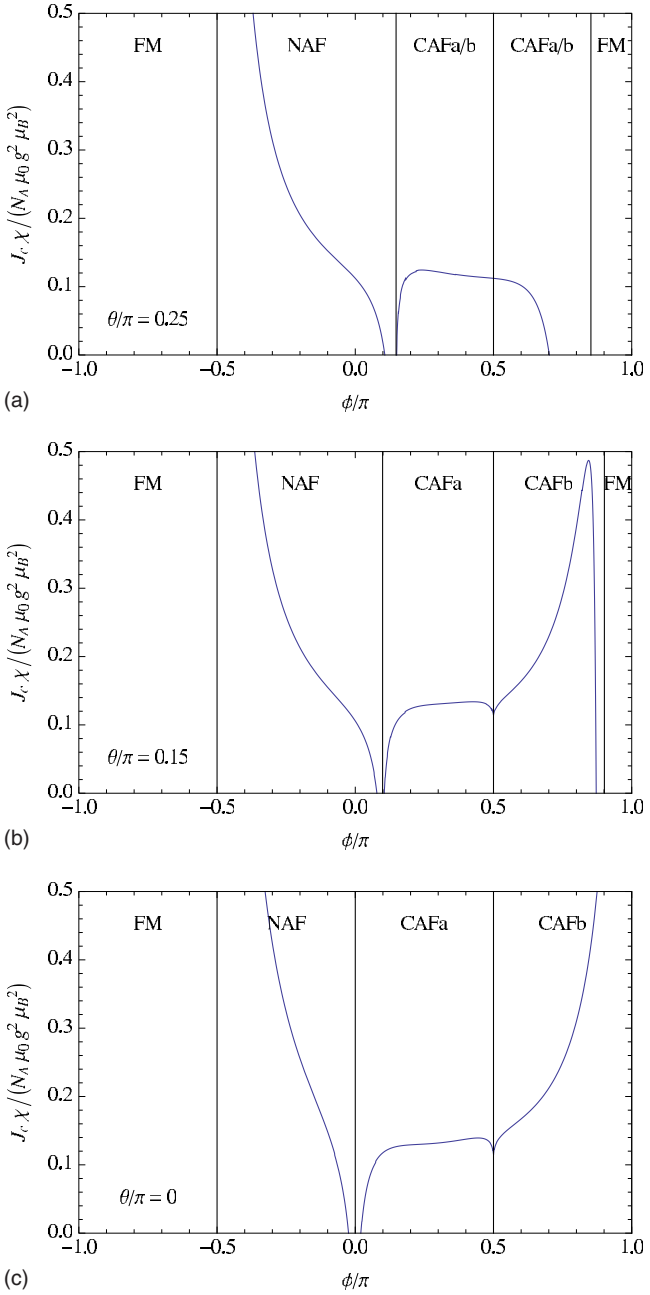

FIG. 8. (Color online) Uniform magnetic susceptibility $\chi = (\partial m/\partial h)_{h\to 0}$ as a function of the frustration angle ϕ for (from top to bottom) $\theta/\pi = 1/4$, $\theta/\pi = 0.15$, and $\theta = 0$.

pockets one would naively expect a constant Pauli susceptibility above the ordering temperature T_m and a reduction below due to the gap opening. While the latter was found for numerous pnictide compounds, the susceptibility above T_m is not constant but still increases roughly linearly with temperature.[36] Explanations for this observation were given within the noninteracting two-band model,[37] an interacting Fermi-liquid picture including nonanalytic correction terms,[38] within a model of coexisting itinerant and localized moments.[17]

On the other hand INS results have shown that low-energy spin excitations can be well described by a suitably parameterized $J_{1a,b}$-J_2 local-moment model according to

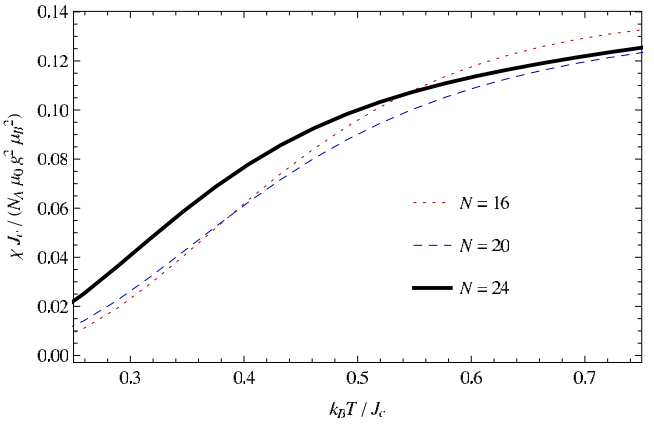

FIG. 9. (Color online) Temperature dependence of the uniform magnetic susceptibility for $\phi/\pi = 0.35$, and $\theta = 0.25$ as for (B) in Table I with $J_c = 58.5$ meV, corresponding to a temperature variation between 170 and 510 K.

Table I. Then one should expect something similar for the low- (zero-) frequency susceptibility, at least qualitatively. To check this conjecture we performed finite-temperature Lanczos calculations as, e.g., described in Ref. 35 for various finite $J_{1a,b}$-J_2 clusters. The result is shown in Fig. 9 for a parameter set (B) corresponding to $BaFe_2As_2$. For temperatures $T \lesssim 0.25 J_c$ the calculation becomes unreliable due to finite-size effects. The temperature range corresponds to ~170 K at the lower and ~510 K at the upper boundary. The increase linearity in T observed for $BaFe_2As_2$ from 150 to 300 K is qualitatively reproduced although the absolute increase is too large. We mention that in the combined itinerant-localized model of Ref. 17 the increased linear T dependence was also attributed to the local-moment contribution. At the very least our calculation shows clearly that in the present range of measurement one should *not* yet expect the high-temperature Curie law $\chi(T) \sim 1/T$ for local-moment systems. This should be expected only quite above the maximum temperature for $\chi(T)$, which is at about $1.1 J_c$ or 750 K in the case of Fig. 9.

VI. SUMMARY AND CONCLUSION

The local-moment model for Fe pnictides has been surprisingly useful to explain the low-energy spin excitations obtained in INS phenomenologically, albeit with the assumption of possibly very anisotropic exchange. The latter may have its microscopic origin in underlying orbital order as proposed in Refs. 12 and 26 but this is still unexplored. The very usefulness of the local-moment picture may be a consequence of Hund's rule correlations in the multiorbital state of Fe pnictides.[12]

In this work we have investigated in detail the empirical localized moment $J_{1a,b}$-J_2 model, in particular, the effect of the in-plane anisotropy and the frustration effect. It has been a recurrent topic to explain the comparatively small ordered moments in Fe pnictides as the effect of enhanced quantum fluctuations in the ground state due to large degeneracy caused by frustrated $J_{1a,b}$ and J_2 exchange bonds.

We have investigated this question in detail using spin-wave approximation and in part the exact-diagonalization Lanczos method to calculate ground-state energy, phase diagram, and moment reduction by quantum fluctuation as function of anisotropy and frustration parameters. In addition we have studied high-field magnetization and low-field uniform susceptibility.

We found that generally the anisotropy lifts the degeneracy between CAFa/b phases and extends their stability range as a function of frustration. Furthermore the anisotropy reduces or closes the instability gap on the phase boundary to the NAF or FM phase, respectively. Most importantly we have shown that in the CAFa sector relevant for the pnictides according to Table I the moment reduction by quantum fluctuations is generally less than for the simple unfrustrated nn Néel antiferromagnet. The same result can be obtained from the uniform low-field susceptibility.

Therefore we conclude that the anomalously low moment in the pnictides is not explained by quantum fluctuations in effective localized moment models but needs a more microscopic viewpoint including the itinerant multiorbital nature of the magnetic state. Such proposals have been made within recent *ab initio* calculations using the full orbital basis.[39–41] This does not invalidate, however, the exceptional usefulness of the simple $J_{1a,b}$-J_2 model to describe the low-energy spin excitations.

We have also derived the spin-wave excitations in an external field for the anisotropic model. It remains to be seen whether new information on the exchange models can be gained from INS experiments in finite fields.

Finally, in a corollary we address a result of our analysis not immediately relevant for pnictides because it is related to the magnetic instability at the CAFa/b-FM boundary ($\phi/\pi = 0.852$). There are 2D local-moment compounds[34] where the frustration angle is quite close to that boundary, contrary to the Fe pnictides. It has been shown for the isotropic model that the true ground state in this region is of the spin-nematic hidden order state.[42] Although spin-wave theory is not adequate to fully address this question we have shown (Fig. 5) that the columnar order at the boundary recovers immediately when turning on even a tiny anisotropy of nn exchange constants $J_{1a,b}$. Since small anisotropies usually exist in such compounds we predict that the spin nematic state of the isotropic J_1-J_2 model will be very hard to find in a real compound.

APPENDIX A: LINEAR SPIN-WAVE ANALYSIS

The formal procedures described here closely follow and generalize those discussed in Refs. 43 and 44, where linear spin-wave theory has been applied to the triangular lattice. In the sections of this appendix, we do not make any assumptions about lattice geometry, dimensionality, and exchange constants except from the requirement that U(1) symmetry is conserved and still exists upon switching on a magnetic field. The Hamiltonian is assumed to have the general form given by Eqs. (1) and (2).

Dropping the primes (working in the local coordinate system), we use boson operators a_i and $a_i^\dagger$ and write

$$S_i^z = S - a_i^\dagger a_i,$$

$$S_i^+ = \sqrt{2S}\left(1 - \frac{a_i^\dagger a_i}{2S}\right)^{1/2} \quad a_i \to \sqrt{2S}a_i,$$

$$S_i^- = \sqrt{2S}a_i^\dagger\left(1 - \frac{a_i^\dagger a_i}{2S}\right)^{1/2} \to \sqrt{2S}a_i^\dagger,$$

$$S_i^x = \frac{1}{2}(S_i^+ + S_i^-) \to \sqrt{\frac{S}{2}}(a_i + a_i^\dagger),$$

$$S_i^y = \frac{1}{2i}(S_i^+ - S_i^-) \to -i\sqrt{\frac{S}{2}}(a_i - a_i^\dagger).$$

Keeping only terms up to bilinear order in the boson operators, we expand the scalar products in Eq. (1). The Hamiltonian up to bilinear order then reads

$$\begin{aligned}\mathcal{H} \to \mathcal{H}_{\rm cl} + \frac{S}{2}\sum_{\langle ij\rangle} &\{(a_i^\dagger a_j + a_i a_j^\dagger)[J_{ij}^\perp \cos(\vec{Q}\vec{R}_{ij})(\cos^2\Theta + 1) + J_{ij}^z \sin^2\Theta] + (a_i a_j + a_i^\dagger a_j^\dagger)[J_{ij}^\perp \cos(\vec{Q}\vec{R}_{ij})(\cos^2\Theta - 1) + J_{ij}^z \sin^2\Theta] \\ &- 2(a_i^\dagger a_i + a_j^\dagger a_j)[J_{ij}^\perp \cos(\vec{Q}\vec{R}_{ij})\sin^2\Theta + J_{ij}^z \cos^2\Theta] - 2i(a_i^\dagger a_j - a_i a_j^\dagger)J_{ij}^\perp \sin(\vec{Q}\vec{R}_{ij})\cos\Theta \\ &- i\sqrt{2S}(a_i - a_i^\dagger - a_j + a_j^\dagger)J_{ij}^\perp \sin(\vec{Q}\vec{R}_{ij})\sin\Theta + \sqrt{2S}(a_i + a_i^\dagger + a_j + a_j^\dagger)[J_{ij}^z - J_{ij}^\perp \cos(\vec{Q}\vec{R}_{ij})]\cos\Theta \sin\Theta\} \\ &+ h\sum_i \left[a_i^\dagger a_i \cos\Theta - \sqrt{\frac{S}{2}}(a_i + a_i^\dagger)\sin\Theta\right].\end{aligned}$$

In the above sum, the contribution

$$\frac{S}{2}\sum_{\langle ij\rangle}[-i\sqrt{2S}(a_i - a_i^\dagger - a_j + a_j^\dagger)J_{ij}^\perp \sin(\vec{Q}\vec{R}_{ij})\sin\Theta]$$

is antisymmetric in the variables i and j (site indices) and therefore vanishes upon summation.

Inserting a Fourier representation of the spin-wave operators $a_i^\dagger$ into the above equation, replacing the sum over bonds $\langle ij\rangle$ with a sum over sites i plus their neighbors n gives after some rearrangement

$$\mathcal{H}-\mathcal{H}_{\mathrm{cl}}=\sqrt{2NS}\sin\Theta\left\{S\cos\Theta\frac{1}{2}\sum_n[J_n^z-J_n^\perp\cos(\vec{Q}\vec{R}_n)]-\frac{h}{2}\right\}(a_0+a_0^\dagger)$$
$$+\frac{S}{2}\sum_{\vec{k}}\frac{1}{2}\sum_n e^{-i\vec{k}\vec{R}_n}\Big(\{J_n^z+J_n^\perp\cos(\vec{Q}\vec{R}_n)-\cos^2\Theta[J_n^z-J_n^\perp\cos(\vec{Q}\vec{R}_n)]\}(a_{\vec{k}}^\dagger a_{\vec{k}}+a_{-\vec{k}}a_{-\vec{k}}^\dagger)$$
$$+[J_n^z-J_n^\perp\cos(\vec{Q}\vec{R}_n)-\cos^2\Theta(J_n^z-J_n^\perp\cos(\vec{Q}\vec{R}_n))](a_{\vec{k}}a_{-\vec{k}}+a_{\vec{k}}^\dagger a_{-\vec{k}}^\dagger)+\frac{2}{i}J_n^\perp\sin(\vec{Q}\vec{R}_n)\cos\Theta(a_{\vec{k}}^\dagger a_{\vec{k}}-a_{-\vec{k}}a_{-\vec{k}}^\dagger)\Big)$$
$$+\frac{S}{2}\sum_{\vec{k}}\frac{1}{2}\sum_n\{-2J_n^\perp\cos(\vec{Q}\vec{R}_n)-2\cos^2\Theta[J_n^z-J_n^\perp\cos(\vec{Q}\vec{R}_n)]\}(a_{\vec{k}}^\dagger a_{\vec{k}}+a_{\vec{k}}a_{\vec{k}}^\dagger-1)+\frac{h}{2}\cos\Theta\sum_{\vec{k}}(a_{\vec{k}}^\dagger a_{\vec{k}}+a_{\vec{k}}a_{\vec{k}}^\dagger-1).$$

Performing the sum over the neighbors n, together with Eqs. (7), (8), (17), and (18) eventually leads to Eq. (16).

We define

$$\hat{a}_{\vec{k}}^\dagger=(a_{\vec{k}}^\dagger,a_{-\vec{k}})$$

to write

$$\mathcal{H}=NS(S+1)[J_\perp(\vec{Q})+A(0)\cos^2\Theta]-\frac{1}{2}Nh(2S+1)\cos\Theta+\frac{S}{2}\sum_{\vec{k}}\hat{a}_{\vec{k}}^\dagger H_{\vec{k}}\hat{a}_{\vec{k}},$$

$$H_{\vec{k}}=\begin{pmatrix}H_1+H_{\mathrm{a}} & H_2\\ H_2 & H_1-H_{\mathrm{a}}\end{pmatrix},$$

$$H_1=A(\vec{k})-\cos^2\Theta[B(\vec{k})+2A(0)]+\frac{h}{S}\cos\Theta,$$

$$H_2=B(\vec{k})(1-\cos^2\Theta_{\mathrm{c}}),$$

$$H_{\mathrm{a}}=C(\vec{k})\cos\Theta,$$

dropping the part linear in $\{a_{\vec{k}=0}^\dagger,a_{\vec{k}=0}\}$. Since the operators $a_{\vec{k}}$ are bosons, their commutation relations can be written as $\hat{a}_{\vec{k}}^\dagger\sigma_z\hat{a}_{\vec{k}}=1$, where σ_z is the symplectic unit matrix (which in our case is identical to the z Pauli spin matrix). Assume $U_{\vec{k}}$ is the matrix which diagonalizes Hamiltonian. From the requirement that this transformation respects the canonical commutation relations, it follows that $U_{\vec{k}}$ must be symplectic, too,

$$U_{\vec{k}}^\dagger\sigma_z U_{\vec{k}}=\sigma_z,$$

and we have

$$U_{\vec{k}}^\dagger\sigma_z H_{\vec{k}}U_{\vec{k}}=\sigma_z D,$$

where D is the diagonal form of $H_{\vec{k}}$. From this transformation, we get the eigenvalues of

$$\sigma_z H_{\vec{k}}=\begin{pmatrix}H_1+H_{\mathrm{a}} & H_2\\ -H_2 & -H_1+H_{\mathrm{a}}\end{pmatrix}$$

by evaluating the characteristic polynomial $\chi(E)=\det(\sigma_z H_{\vec{k}}-E)$. This polynomial can always be written as

$$\chi(E)=\det[(E-H_{\mathrm{a}})^2-(H_1-H_2)(H_1+H_2)],$$

and the desired spin-wave dispersion can be immediately read off,

$$E(h,\vec{k})=\sqrt{(H_1-H_2)(H_1+H_2)}+H_{\mathrm{a}}$$
$$=\left\{\left[A(\vec{k})-B(\vec{k})-2A(0)\cos^2\Theta+\frac{h}{S}\cos\Theta\right]\times\left[A(\vec{k})+B(\vec{k})(1-2\cos^2\Theta)-2A(0)\cos^2\Theta+\frac{h}{S}\cos\Theta\right]\right\}^{1/2}+C(\vec{k})\cos\Theta$$
$$=\sqrt{\left\{A(\vec{k})-\cos^2\Theta[B(\vec{k})+2A(0)]+\frac{h}{S}\cos\Theta\right\}^2-[B(\vec{k})(1-\cos^2\Theta)]^2}+C(\vec{k})\cos\Theta,$$

where we have taken the root with the positive sign only. Setting $\Theta=\Theta_{\mathrm{c}}$ eventually leads to the dispersion, Eq. (23).

APPENDIX B: ORDERED MOMENT

Writing the Hamiltonian, Eq. (16), with the spin-wave operators $\alpha_{\vec{k}}^{\dagger}$, Eqs. (21) and (22), and diagonalizing the LSW Hamiltonian in a more explicit way we get

$$u_{\vec{k}} = \text{sign}\, B(\vec{k}) \sqrt{\frac{1}{2}\left\{\frac{A(\vec{k}) - \cos^2\Theta[B(\vec{k}) + 2A(0)] + \frac{h}{S}\cos\Theta}{E(h,\vec{k})} + 1\right\}},$$

$$v_{\vec{k}} = \sqrt{\frac{1}{2}\left\{\frac{A(\vec{k}) - \cos^2\Theta[B(\vec{k}) + 2A(0)] + \frac{h}{S}\cos\Theta}{E(h,\vec{k})} - 1\right\}}.$$

Setting $\Theta = \Theta_c$ and inserting the coefficients $v_{\vec{k}}$ into Eq. (31) yields the expression (32) for the ordered moment.

APPENDIX C: UNIFORM MOMENT AND SUSCEPTIBILITY

The uniform moment is given by Eq. (35), or equivalently

$$m = -\frac{1}{N}\frac{\partial E_{gs}(\Theta_c)}{\partial \cos\Theta_c}\frac{\partial \cos\Theta_c}{\partial h} \tag{C1}$$

with the ground-state energy in linear spin-wave approximation

$$E_{gs}(\Theta_c) = NS^2[J_\perp(\vec{Q}) - A(0)\cos^2\Theta_c] + NSJ_\perp(\vec{Q}) + \frac{S}{2}\sum_{\vec{k}} E(h,\vec{k}),$$

and $E(h,\vec{k})$ given by Eq. (23). We have

$$\frac{\partial E_{gs}(\Theta_c)}{\partial \cos\Theta_c} = -2A(0)\cos\Theta_c + \frac{S}{2}\sum_{\vec{k}}\frac{\partial E(h,\vec{k})}{\partial \cos\Theta_c},$$

$$\frac{\partial \cos\Theta_c}{\partial h} = \frac{1}{2SA(0)},$$

$$\frac{\partial E(h,\vec{k})}{\partial \cos\Theta_c} = -2\cos\Theta_c\frac{B(\vec{k})[A(\vec{k}) - B(\vec{k})]}{E(h,\vec{k})},$$

Inserting these expressions into Eq. (C1) gives the desired result, Eq. (36).

The correction to the magnetization [the deviation from the classical behavior $m_{cl} = S\cos\Theta_c = S(h/h_s)$] at this level of approximation is a consequence of the zero-point fluctuations only. Integrating Eq. (35) between $h=0$ and $h=h_s$, we can write

$$\Delta E_{gs} = E_{gs}(h = h_s) - E_{gs}(h = 0) = -N\int_0^{h_s} m(h)dh. \tag{C2}$$

As discussed elsewhere, the zero-point fluctuations reduce $E_{gs}(h=0)$, but do not reduce $E_{gs}(h_s)$. For the latter, the zero-point fluctuations vanish, again because the fully polarized state at h_s is an eigenstate of $\mathcal{H}$. Thus the classical energy difference is smaller than the energy difference including first-order corrections in Eq. (C2),

$$\begin{aligned}\Delta E_{gs}^{cl} - \Delta E_{gs}^{LSW} &= E_{gs}^{cl}(h_s) - E_{gs}^{cl}(0) - [E_{gs}^{LSW}(h_s) - E_{gs}^{LSW}(0)] \\ &= E_{gs}^{LSW}(0) - E_{gs}^{cl}(0) = NSJ_\perp(\vec{Q}) + \frac{S}{2}\sum_{\vec{k}} E(\vec{k}) \\ &= E_{zp} \le 0,\end{aligned}$$

hence the corrections to the integrated magnetization must be negative. Assuming a monotonic behavior of $m(h)$, the same relation holds for the kernel in Eq. (C2), and it follows that

$$m_{LSW}(h) \le m_{cl}(h), \quad h \le h_s,$$

consequently we can expect that the corrected magnetization curve lies below the classical one.

For the susceptibility, we differentiate m once more with respect to the applied field,

$$\chi = \frac{\partial m}{\partial \cos\Theta_c}\frac{\partial \cos\Theta_c}{\partial h},$$

and using

$$\frac{\partial m}{\partial \cos\Theta_c} = \frac{m}{\cos\Theta_c} + S\cos\Theta_c \frac{1}{2S}\frac{1}{N}\sum_{\vec{k}}\left\{-\frac{B(\vec{k})[A(\vec{k})-B(\vec{k})]}{A(0)E^2(h,\vec{k})}\frac{\partial E(h,\vec{k})}{\partial\cos\Theta_c}\right\}$$

$$= S\left\{1+\frac{1}{2S}\frac{1}{N}\sum_{\vec{k}}\frac{B(\vec{k})[A(\vec{k})-B(\vec{k})]}{A(0)E(h,\vec{k})} + \cos^2\Theta_c\frac{1}{S}\frac{1}{N}\sum_{\vec{k}}\frac{B^2(\vec{k})[A(\vec{k})-B(\vec{k})]^2}{A(0)E^3(h,\vec{k})}\right\}.$$

We obtain Eq. (37).

[1] W. L. Yang *et al.*, Phys. Rev. B **80**, 014508 (2009).
[2] K. Kaneko, A. Hoser, N. Caroca-Canales, A. Jesche, C. Krellner, O. Stockert, and C. Geibel, Phys. Rev. B **78**, 212502 (2008).
[3] T. Yildirim, Phys. Rev. Lett. **101**, 057010 (2008).
[4] A. N. Yaresko, G.-Q. Liu, V. N. Antonov, and O. K. Andersen, Phys. Rev. B **79**, 144421 (2009).
[5] M. J. Han, Q. Yin, W. E. Pickett, and S. Y. Savrasov, Phys. Rev. Lett. **102**, 107003 (2009).
[6] R. A. Ewings, T. G. Perring, R. I. Bewley, T. Guidi, M. J. Pitcher, D. R. Parker, S. J. Clarke, and A. T. Boothroyd, Phys. Rev. B **78**, 220501(R) (2008).
[7] R. J. McQueeney *et al.*, Phys. Rev. Lett. **101**, 227205 (2008).
[8] J. Zhao *et al.*, Phys. Rev. Lett. **101**, 167203 (2008).
[9] S. O. Diallo *et al.*, Phys. Rev. Lett. **102**, 187206 (2009).
[10] J. Zhao, D. T. Adroja, D.-X. Yao, R. Bewley, S. Li, X. F. Wang, G. Wu, X. H. Chen, J. Hu, and P. Dai, Nat. Phys. **5**, 555 (2009).
[11] Z. P. Yin, S. Lebegue, M. J. Han, B. P. Neal, S. Y. Savrasov, and W. E. Pickett, Phys. Rev. Lett. **101**, 047001 (2008).
[12] S. Zhou and Z. Wang, arXiv:0910.2707 (unpublished).
[13] G. Stollhoff and P. Thalmeier, Z. Phys. B: Condens. Matter **43**, 13 (1981).
[14] A. M. Oleś, Phys. Rev. B **23**, 271 (1981).
[15] M. F. Collins, V. J. Minkiewicz, R. Nathans, L. Passell, and G. Shirane, Phys. Rev. **179**, 417 (1969).
[16] H. Zhai, F. Wang, and D.-H. Lee, Phys. Rev. B **80**, 064517 (2009).
[17] S.-P. Kou, T. Li, and Z.-Y. Weng, EPL **88**, 17010 (2009).
[18] L. de'Medici, S. Hassan, and M. Capone, J. Supercond. Novel Magn. **22**, 535 (2009).
[19] F. Krüger, S. Kumar, J. Zaanen, and J. van den Brink, Phys. Rev. B **79**, 054504 (2009); W. Lv, F. Krüger, and P. Philips, arXiv:1002.3165 (unpublished).
[20] C.-C. Chen, B. Moritz, J. van den Brink, T. P. Devereaux, and R. R. P. Singh, Phys. Rev. B **80**, 180418(R) (2009).
[21] Q. Si and E. Abrahams, Phys. Rev. Lett. **101**, 076401 (2008).
[22] J. P. Rodriguez and E. H. Rezayi, Phys. Rev. Lett. **103**, 097204 (2009); J. P. Rodriguez, arXiv:1002.0891 (unpublished).
[23] R. Yu, K. T. Trinh, A. Moreo, M. Daghofer, J. A. Riera, S. Haas, and E. Dagotto, Phys. Rev. B **79**, 104510 (2009).
[24] I. Eremin and A. Chubukov, Phys. Rev. B **81**, 024511 (2010).
[25] H. Lee, Y. Zhang, H. Jeschke, and R. Valenti, arXiv:0912.4024 (unpublished).
[26] K. Kubo and P. Thalmeier, J. Phys. Soc. Jpn. **78**, 083704 (2009).
[27] M. Daghofer, A. Nicholson, A. Moreo, and E. Dagotto, Phys. Rev. B **81**, 014511 (2010).
[28] G. S. Uhrig, M. Holt, J. Oitmaa, O. P. Sushkov, and R. R. P. Singh, Phys. Rev. B **79**, 092416 (2009).
[29] D.-X. Yao and E. W. Carlson, Phys. Rev. B **78**, 052507 (2008).
[30] D. Yao and E. Carlson, arXiv:0910.2528, special issue of Fron. Phys. China (to be published).
[31] A. Smerald and N. Shannon, arXiv:0909.2207 (unpublished).
[32] R. Applegate, J. Oitmaa, and R. R. P. Singh, Phys. Rev. B **81**, 024505 (2010).
[33] B. Schmidt, P. Thalmeier, and N. Shannon, Phys. Rev. B **76**, 125113 (2007).
[34] P. Thalmeier, M. E. Zhitomirsky, B. Schmidt, and N. Shannon, Phys. Rev. B **77**, 104441 (2008).
[35] N. Shannon, B. Schmidt, K. Penc, and P. Thalmeier, Eur. Phys. J. B **38**, 599 (2004).
[36] R. Klingeler, N. Leps, I. Hellmann, A. Popa, U. Stockert, C. Hess, V. Kataev, H. Grafe, F. Hammerath, G. Lang, G. Behr, L. Harnagea, S. Singh, and B. Buechner, Phys. Rev. B **81**, 024506 (2010).
[37] B. C. Sales, M. A. McGuire, A. S. Sefat, and D. Mandrus, Physica C **470**, 304 (2010).
[38] M. M. Korshunov, I. Eremin, D. V. Efremov, D. L. Maslov, and A. V. Chubukov, Phys. Rev. Lett. **102**, 236403 (2009).
[39] F. Cricchio, O. Granäs, and L. Nordström, arXiv:0911.1342 (unpublished).
[40] C.-C. Lee, W.-G. Yin, and W. Ku, Phys. Rev. Lett. **103**, 267001 (2009).
[41] Y. Zhang, I. Opahle, H. Jeschke, and R. Valenti, Phys. Rev. B **81**, 094505 (2010).
[42] N. Shannon, T. Momoi, and P. Sindzingre, Phys. Rev. Lett. **96**, 027213 (2006).
[43] T. Ohyama and H. Shiba, J. Phys. Soc. Jpn. **63**, 3454 (1994).
[44] M. Y. Veillette, J. T. Chalker, and R. Coldea, Phys. Rev. B **71**, 214426 (2005).